Multibody System Dynamics

Electronic supplementary material for On the modeling of the intervertebral joint in multibody models for the spine: *Review of Stiffness Matrices for the Intervertebral Joint*

Miguel Christophy · Maurice Curtin · Nur Adila Faruk Senan · Jeffrey C. Lotz · Oliver M. O'Reilly

December 3, 2011

Summary This supplemental work to Christophy et al. "On the modeling of the intervertebral joint in multibody models for the spine" *Multibody System Dynamics*, Vol. 30, No. 4, 413-432 (2013) reviews various formulations of stiffness matrices that can be used in conjunction with the relative motion of a pair of rigid bodies. Particular attention is paid to the application of these matrices to models of the intervertebral joint. To make the presentation as self contained as possible, relevant background from the kinematics of rigid bodies and the 1-2-3 set of Euler angles are also provided.

Miguel Christophy · Nur Adila Faruk Senan · Oliver M. O'Reilly
Department of Mechanical Engineering,
University of California at Berkeley,
Berkeley, CA 94720-1740
USA
Tel.: +510-642-0877
Fax: +510-643-5599
E-mail: christophy@gmail.com
E-mail: adilapapaya@gmail.com
E-mail: oreilly@berkeley.edu

Maurice Curtin
School of Electrical, Electronic and Communications Engineering
University College Dublin
Belfield, Dublin 4,
Ireland
E-mail: moecurtin@gmail.com

Jeffrey C. Lotz
Department of Orthopaedic Surgery,
University of California at San Francisco,
San Francisco, CA 94143-0514
USA
Tel.: +415-476-7881
Fax.: +415-476-1128
E-mail: lotzj@orthosurg.ucsf.edu

1 Introduction to supplemental material

In Christophy et al. [3], a bushing force element for the intervertebral joint is introduced and implemented in an open-source platform that simulates musculoskeletal models. Here, the background information needed to help comprehend this implementation is presented. Much of the material in these notes is an extension of our earlier discussion in [15] on the stiffness matrix of the intervertebral joint. This extension was made possible by the work in [12] on Cartesian stiffness matrices. We mention that, while our exposition here is motivated by the application of the stiffness matrix to the intervertebral joint, it can very easily be extended for modeling other joints in the body such as the knee [1].

An outline of the supplemental material is as follows. First, representations for rigid body motions are presented in Section 2 and background on the 1-2-3 set of Euler angles are presented in Section 3. This material is then applied to parameterize the relative motion of a pair of rigid bodies in Section 4. The formulation of stiffness matrices based on the existence of a potential energy function is discussed in Section 5. Our discussion emphasizes the role that the Euler angle parameterization of the relative rotation of a pair of rigid bodies and the landmarks used to define the relative displacement play in the specification of a stiffness matrix. In Section 6, we relate the stiffness matrices presented in Section 5 to those used in describing the bushing force element in [3] and several stiffness matrices which have appeared in the literature.

The notation used here and in [3] is identical to our earlier work on stiffness matrices [12] and features tensorial notation. Additional background on the latter and its use in rigid body dynamics can be found in the textbook [14]. In the present work, arrays of real

numbers are denoted by san-serif Roman letters, such as T, p, while vectors and tensors are denoted by bold-faced Roman letters, e.g., $\bar{\mathbf{x}}$ and $\mathbf{R}$. Additionally, we reserve capital letter sub- and super-scripts to indicate specific bodies (e.g., bodies $\mathcal{V}_K$, basis vectors $\mathbf{e}_i^K$) while uncapitalized indices are used to specify components of vectors, tensors, and arrays of real numbers, such as ω_i, K_{ij}, q_i, $\tilde{T}_{ij}$.

2 Background on rigid body motions

We first recall that a rigid body $\mathcal{V}$ consists of a collection of material points X where the distance between any of these points remains constant. As shown in Fig. 1, it is convenient to define a fixed reference configuration $\boldsymbol{\kappa}_0$ of this body. This configuration occupies a fixed region of Euclidean three-space $\mathbb{E}^3$. The position vector, relative to a fixed origin O, of a material point X in this configuration is defined by the position vector $\mathbf{X}$. In a similar manner, the present (or current) configuration $\boldsymbol{\kappa}_t$ of $\mathcal{V}$ can be defined and the position vector of a material point X in this configuration is denoted by $\mathbf{x}$. The position vector $\mathbf{x}$ of a point X, which has a position

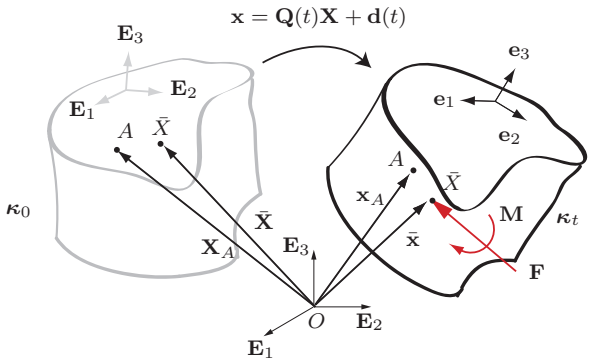

Fig. 1: *The reference $\boldsymbol{\kappa}_0$ and present $\boldsymbol{\kappa}_t$ configurations of a rigid body $\mathcal{V}$ which represents a lumbar vertebra. This figure also displays the corotational basis $\{\mathbf{e}_1, \mathbf{e}_2, \mathbf{e}_3\}$, center of mass $\bar{X}$, material point A, and the resultant force $\mathbf{F}$ and moment $\mathbf{M}$ acting at the center of mass of the vertebra.*

vector $\mathbf{X}$ in $\boldsymbol{\kappa}_0$, has the vector-valued representation

$$\mathbf{x} = \mathbf{Q}(t)\mathbf{X} + \mathbf{d}(t). \tag{S.1}$$

Here, $\mathbf{d}(t)$ is a vector-valued function of time, and $\mathbf{Q}(t)$ is a rotation (or proper-orthogonal) tensor. That is, $\mathbf{Q}\mathbf{Q}^T = \mathbf{I}$ and $\det(\mathbf{Q}) = 1$.

It is convenient to define two right-handed orthonormal bases for $\mathbb{E}^3$: a fixed basis $\{\mathbf{E}_1, \mathbf{E}_2, \mathbf{E}_3\}$ and a corotational (body-fixed) basis $\{\mathbf{e}_1, \mathbf{e}_2, \mathbf{e}_3\}$. The basis vectors are related by the rotation tensor $\mathbf{Q}$:

$$\mathbf{e}_i = \mathbf{Q}\mathbf{E}_i, \qquad (i = 1, 2, 3)\,. \tag{S.2}$$

Of particular interest are the position vector of the center of mass $\bar{X}$ and a landmark point A. These vectors are denoted by $\bar{\mathbf{x}}$ and $\mathbf{x}_A$ respectively. For the position vectors $\bar{\mathbf{x}}$ and $\mathbf{x}_A$, we have the representations

$$\bar{\mathbf{x}} = \sum_{k=1}^{3} X_k \mathbf{E}_k = \sum_{i=1}^{3} x_i \mathbf{e}_i,$$

$$\mathbf{x}_A = \sum_{i=1}^{3} X_{A_i} \mathbf{E}_i = \sum_{k=1}^{3} x_{A_k} \mathbf{e}_k. \tag{S.3}$$

The tensor $\mathbf{Q} = \sum_{i=1}^{3} \mathbf{e}_i \otimes \mathbf{E}_i$ has several equivalent representations:

$$\mathbf{Q} = \sum_{i=1}^{3}\sum_{k=1}^{3} Q_{ik} \mathbf{E}_i \otimes \mathbf{E}_k = \sum_{i=1}^{3}\sum_{k=1}^{3} Q_{ik} \mathbf{e}_i \otimes \mathbf{e}_k, \tag{S.4}$$

where $\otimes$ is the tensor product: $(\mathbf{a} \otimes \mathbf{b})\,\mathbf{c} = (\mathbf{b} \cdot \mathbf{c})\,\mathbf{a}$ for any vectors $\mathbf{a}$, $\mathbf{b}$ and $\mathbf{c}$. Given a vector $\mathbf{a}$ we can establish the following relationships between its components in bases related by a rotation tensor $\mathbf{Q}$:

$$\begin{bmatrix} \mathbf{a}\cdot\mathbf{E}_1 \\ \mathbf{a}\cdot\mathbf{E}_2 \\ \mathbf{a}\cdot\mathbf{E}_3 \end{bmatrix} = \mathsf{Q} \begin{bmatrix} \mathbf{a}\cdot\mathbf{e}_1 \\ \mathbf{a}\cdot\mathbf{e}_2 \\ \mathbf{a}\cdot\mathbf{e}_3 \end{bmatrix}, \text{ where } \mathsf{Q} = \begin{bmatrix} Q_{11} & Q_{12} & Q_{13} \\ Q_{21} & Q_{22} & Q_{23} \\ Q_{31} & Q_{32} & Q_{33} \end{bmatrix}. \tag{S.5}$$

The inverse of the matrix Q is its transpose: $\mathsf{Q}^{-1} = \mathsf{Q}^T$.

3 Euler angle parameterization of a rotation

Recall that the rotation of a rigid body is completely characterized by the rotation tensor $\mathbf{Q}$. Tensors of this type can be parameterized in a variety of manners (see [21]). Of interest here is the Euler angle representation of a rotation tensor whereby the tensor $\mathbf{Q}$ is decomposed into the product of three simple rotations:

$$\mathbf{Q} = \hat{\mathbf{Q}}(\nu_1, \nu_2, \nu_3) = \mathbf{L}(\nu_3, \mathbf{g}_3)\mathbf{L}(\nu_2, \mathbf{g}_2)\mathbf{L}(\nu_1, \mathbf{g}_1), \tag{S.6}$$

where $\mathbf{L}(\nu, \mathbf{g})$ represents a counterclockwise rotation by an angle ν about the unit vector $\mathbf{g}$. The set $\{\mathbf{g}_1, \mathbf{g}_2, \mathbf{g}_3\}$ is known as the Euler basis and define the dual Euler basis vectors $\{\mathbf{g}^1, \mathbf{g}^2, \mathbf{g}^3\}$ using the 9 identities[1]

$$\mathbf{g}_i \cdot \mathbf{g}^j = \delta_i^j. \tag{S.7}$$

[1] Readers who are more familiar with the notation of Kane and his coworkers [10] might recognize the Euler basis as the body-two or body-three basis vectors $\{\mathbf{b}_1, \mathbf{b}_2, \mathbf{b}_3\}$(not to be confused with the set of basis vectors associated with the bushing frames $\mathbb{B}_1$ and $\mathbb{B}_2$).

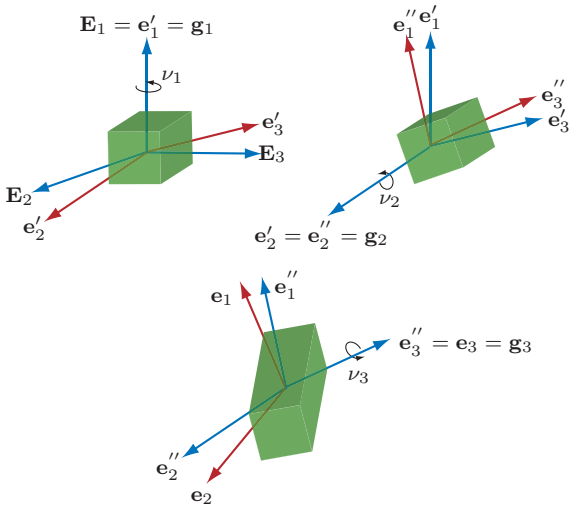

Fig. 2: *The 1-2-3 Euler angle rotation sequence for the rotation tensor* $\mathbf{Q} = \sum_{k=1}^{3} \mathbf{e}_k \otimes \mathbf{E}_k$ *of a rigid body. Here,* $\mathbf{e}'_i$ *and* $\mathbf{e}''_i$ *are the intermediate basis vectors following the respective rotation by* ν_1 *about* $\mathbf{E}_1$ *and* ν_2 *about* $\mathbf{e}'_2$.

One can consider the Euler basis $\{\mathbf{g}_1, \mathbf{g}_2, \mathbf{g}_3\}$ and the dual Euler basis $\{\mathbf{g}^1, \mathbf{g}^2, \mathbf{g}^3\}$ as basis vectors in the tangent and cotangent spaces respectively of the manifold $SO(3)$. Further uses of the dual Euler basis and its relation to constraint moments, moment potentials, and Lagrange's equations of motion are discussed in [13].

Let $\boldsymbol{\omega}$ denote the angular velocity vector associated with $\mathbf{Q}$ as specified by (S.6). Then, we can write three distinct representations for the vector $\boldsymbol{\omega}$:

$$\boldsymbol{\omega} = \sum_{i=1}^{3} \dot{\nu}_i \mathbf{g}_i = \sum_{i=1}^{3} \omega_i \mathbf{e}_i = \sum_{i=1}^{3} \Omega_i \mathbf{E}_i. \tag{S.8}$$

Taking the dot product of (S.8) with $\mathbf{g}^i$ gives

$$\dot{\nu}_i = \sum_{j=1}^{3} \left(({}^{e}\mathsf{T})_{ij}\, \omega_j \right) = \sum_{j=1}^{3} \left(({}^{E}\mathsf{T})_{ij}\, \Omega_j \right), \tag{S.9}$$

where the $()_{ij}$ components of ${}^{e}\mathsf{T}$ and ${}^{E}\mathsf{T}$ are given by [2]

$$({}^{e}\mathsf{T})_{ij} = \mathbf{g}^i \cdot \mathbf{e}_j, \qquad \left({}^{E}\mathsf{T}\right)_{ij} = \mathbf{g}^i \cdot \mathbf{E}_j. \tag{S.10}$$

Conversely, the components of $\boldsymbol{\omega}$ in the fixed and moving frames can be determined by dotting into the $\mathbf{E}_i$ and $\mathbf{e}_i$ basis vectors respectively to obtain

$$\Omega_i = \sum_{j=1}^{3} \left({}^{E}\mathsf{W}\right)_{ij} \dot{\nu}_j, \qquad \omega_i = \sum_{j=1}^{3} ({}^{e}\mathsf{W})_{ij}\, \dot{\nu}_j. \tag{S.11}$$

[2] The matrix ${}^{E}\mathsf{W}$ is equivalent to the matrix $\mathbf{G}^i$ while ${}^{e}\mathsf{W}$ is equivalent to the matrix $\bar{\mathbf{G}}^i$ in the multibody dynamics literature (see, e.g., Shabana [20]).

Here,

$$({}^{e}\mathsf{W})_{ij} = \mathbf{e}_i \cdot \mathbf{g}_j, \qquad \left({}^{E}\mathsf{W}\right)_{ij} = \mathbf{E}_i \cdot \mathbf{g}_j. \tag{S.12}$$

Identity (S.7) can be used in combination with expressions (S.10) and (S.12) to show that

$$({}^{e}\mathsf{T})\,({}^{e}\mathsf{W}) = \mathsf{I}, \qquad \left({}^{E}\mathsf{T}\right)\left({}^{E}\mathsf{W}\right) = \mathsf{I}. \tag{S.13}$$

Among the 12 possible sets of Euler angle sequences of particular interest in the present paper is the 1-2-3 set. As can be seen from Fig. 2, for this choice of Euler angles

$$\mathbf{g}_1 = \mathbf{E}_1, \qquad \mathbf{g}_2 = \mathbf{e}'_2 = \cos(\nu_1)\mathbf{E}_2 + \sin(\nu_1)\mathbf{E}_3,$$
$$\mathbf{g}_3 = \mathbf{e}_3 = \cos(\nu_2)\mathbf{e}'_3 + \sin(\nu_2)\mathbf{e}'_1. \tag{S.14}$$

Further the matrices ${}^{e}\mathsf{T}$ and ${}^{e}\mathsf{W}$ are

$${}^{e}\mathsf{T} = \begin{bmatrix} \cos(\nu_3)\sec(\nu_2) & -\sin(\nu_3)\sec(\nu_2) & 0 \\ \sin(\nu_3) & \cos(\nu_3) & 0 \\ -\cos(\nu_3)\tan(\nu_2) & \sin(\nu_3)\tan(\nu_2) & 1 \end{bmatrix}, \tag{S.15}$$

$${}^{e}\mathsf{W} = \begin{bmatrix} \cos(\nu_2)\cos(\nu_3) & \sin(\nu_3) & 0 \\ -\cos(\nu_2)\sin(\nu_3) & \cos(\nu_3) & 0 \\ \sin(\nu_2) & 0 & 1 \end{bmatrix}. \tag{S.16}$$

We note that all 24 ${}^{e}\mathsf{T}$ and ${}^{e}\mathsf{W}$ matrices (one for each of the possible Euler angle combinations) can be inferred from the representations of ω_i and $\dot{\nu}_i$ given in Appendix II of [10]. Additionally, the matrices ${}^{E}\mathsf{T}$ and ${}^{E}\mathsf{W}$ are related to the matrices ${}^{e}\mathsf{T}$ and ${}^{e}\mathsf{W}$ specified in (S.15) and (S.16) by the rotation matrix Q (cf. (S.5)):

$${}^{E}\mathsf{T} = ({}^{e}\mathsf{T})\,\mathsf{Q}^T = \begin{bmatrix} 1 & \tan(\nu_2)\sin(\nu_1) & -\tan(\nu_2)\cos(\nu_1) \\ 0 & \cos(\nu_1) & \sin(\nu_1) \\ 0 & -\sin(\nu_1)\sec(\nu_2) & \cos(\nu_1)\sec(\nu_2) \end{bmatrix}, \tag{S.17}$$

$${}^{E}\mathsf{W} = \mathsf{Q}\,({}^{e}\mathsf{W}) = \begin{bmatrix} 1 & 0 & \sin(\nu_2) \\ 0 & \cos(\nu_1) & -\cos(\nu_2)\sin(\nu_1) \\ 0 & \sin(\nu_1) & \cos(\nu_2)\cos(\nu_1) \end{bmatrix}. \tag{S.18}$$

As anticipated, ${}^{E}\mathsf{W} = {}^{E}\mathsf{T}^{-1}$.

4 Application to a pair of rigid bodies

Suppose that the system of interest is composed of two rigid bodies in relative motion (as in the motion of the fourth lumber vertebra relative to the fifth lumber vertebra (Fig. 3)). In this case, it is often convenient to define the motion of the second body with respect to the motion of the first body. To this end, we pick a single material point on each body, X_A^1 and X_A^2, and denote the position vectors of these landmarks by $\mathbf{x}_A^1$

and $\mathbf{x}_A^2$, respectively. We emphasize that it is not necessary to assume that the landmarks correspond to the centers of mass $\bar{X}^1$ and $\bar{X}^2$ of the bodies. We denote the rotation tensor associated with the K^{th} body by $\mathbf{Q}_K$ where $K = 1, 2$ respectively. We can now define

$$\mathbf{y}_A = \mathbf{x}_A^2 - \mathbf{x}_A^1 = \sum_{i=1}^{3} Y_i \mathbf{E}_i \tag{S.19}$$

as the relative position vector between the landmarks on the two bodies while

$$\mathbf{R} = \mathbf{Q}_2 \mathbf{Q}_1^T \tag{S.20}$$

is the relative rotation tensor. It is also convenient to introduce the corotational basis vectors $\mathbf{e}_i^K = \mathbf{Q}_K \mathbf{E}_i$ (depicted on the bodies $\mathcal{V}_2$ and $\mathcal{V}_1$ in Fig. 3) associated with the Kth body.

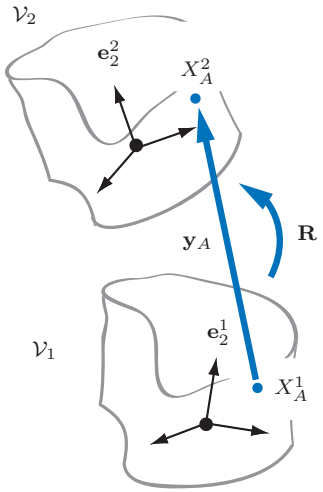

Fig. 3: *The relative motion between the landmarks X_A^1 and X_A^2 situated on the $\mathcal{V}_1$ and $\mathcal{V}_2$ bodies respectively can be represented using the displacement vector $\mathbf{y}_A$ and rotation tensor $\mathbf{R}$.*

We parameterize $\mathbf{R}$ and $\mathbf{Q}_K$ by the relative and absolute Euler angle sets $\{\beta_1, \beta_2, \beta_3\}$ and $\{\nu_1^K, \nu_2^K, \nu_3^K\}$. Thus,

$$\boldsymbol{\omega}^K = \dot{\nu}_1^K \mathbf{g}_1^K + \dot{\nu}_2^K \mathbf{g}_2^K + \dot{\nu}_3^K \mathbf{g}_3^K \tag{S.21}$$

is the angular velocity of body K and

$$\tilde{\boldsymbol{\omega}} = \boldsymbol{\omega}^2 - \boldsymbol{\omega}^1 = \dot{\beta}_1 \tilde{\mathbf{g}}_1 + \dot{\beta}_2 \tilde{\mathbf{g}}_2 + \dot{\beta}_3 \tilde{\mathbf{g}}_3 \tag{S.22}$$

is the relative angular velocity vector. In these equations, $\{\mathbf{g}_1^K, \mathbf{g}_2^K, \mathbf{g}_3^K\}$ is the Euler basis (with dual basis $\{\mathbf{g}^{K,1}, \mathbf{g}^{K,2}, \mathbf{g}^{K,3}\}$) of the K^{th} rigid body, and $\{\tilde{\mathbf{g}}_1, \tilde{\mathbf{g}}_2, \tilde{\mathbf{g}}_3\}$ is the Euler basis of the relative rotation between the second and first body. This third Euler basis has an associated dual Euler basis $\{\tilde{\mathbf{g}}^1, \tilde{\mathbf{g}}^2, \tilde{\mathbf{g}}^3\}$. In the paper, the tensor $\mathbf{R}$ is parameterized using a set of 1-2-3 Euler angles.

In spinal mechanics, one of the more common choices of the landmark points X_A^K are the vertebral centers of geometry but one can also opt to use other landmarks such as points on the upper and lower vertebral surfaces [5,7,17,22,23]. Of particular importance is to note that, if these, or other, experimental data are used to populate stiffness matrices it is crucial to identify the landmark material points X_A^1 and X_A^2 associated with the relative displacement $\mathbf{y}_A$ and to accommodate any possible differences in the choices of Euler angles and basis vectors.

5 Stiffness matrices and potential energy

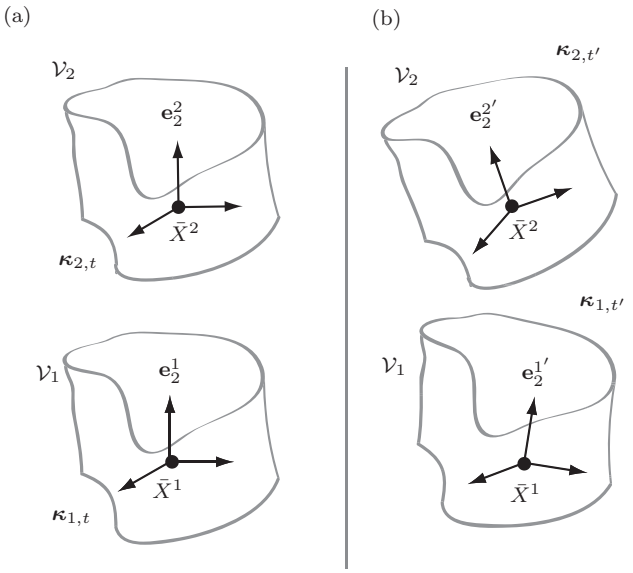

Fig. 4: *The configurations $\boldsymbol{\kappa}_{1,t}$ and $\boldsymbol{\kappa}_{2,t}$ of $\mathcal{V}_1$ and $\mathcal{V}_2$, respectively, are depicted in (a). As shown in (b), both bodies then undergo an infinitesimal relative rigid body motion and occupy the configurations $\boldsymbol{\kappa}_{1,t'}$ and $\boldsymbol{\kappa}_{2,t'}$. Also shown in this figure are the corotational basis vectors $\{\mathbf{e}_1^1, \mathbf{e}_2^1, \mathbf{e}_3^1\}$ and $\{\mathbf{e}_1^2, \mathbf{e}_2^2, \mathbf{e}_3^2\}$ which are attached to the $\mathcal{V}_1$ and $\mathcal{V}_2$ bodies respectively.*

Consider a pair of rigid bodies, $\mathcal{V}_1$ and $\mathcal{V}_2$ such as those shown in Fig. 3. We assume that the forces and moments exerted by the pair of bodies due to their mutual interaction are conservative. As a result, we can define a potential energy function U:

$$U = U(Y_1, Y_2, Y_3, \beta_1, \beta_2, \beta_3). \tag{S.23}$$

Then, following the methodology used in [12,16], expressions for the conservative forces $\mathbf{F}_1^A$ and $\mathbf{F}_2^A$ and conservative moments $\mathbf{M}_1^A$ and $\mathbf{M}_2^A$ can be computed:

$$\mathbf{F}_2^A = -\mathbf{F}_1^A = \sum_{i=1}^{3} \left(-\frac{\partial U}{\partial Y_i} \mathbf{E}_i \right),$$

$$\mathbf{M}_2^A = -\mathbf{M}_1^A = \sum_{i=1}^{3} \left(-\frac{\partial U}{\partial \beta_i} \tilde{\mathbf{g}}^i \right). \tag{S.24}$$

The force $\mathbf{F}_1^A$ is the force exerted on $\mathcal{V}_1$ at X_A^1, the force $\mathbf{F}_2^A$ is the force exerted on $\mathcal{V}_2$ at X_A^2, the moment $\mathbf{M}_1^A$ is relative to the material point X_A^1 of $\mathcal{V}_1$, and the moment $\mathbf{M}_2^A$ is relative to the material point X_A^2 of $\mathcal{V}_2$.

We also take this opportunity to introduce the notation $\mathbf{F}_1$ and $\mathbf{M}_1$ for the forces and moments exerted at the center of mass $\bar{X}^1$ of $\mathcal{V}_1$ and $\mathbf{F}_2$ and $\mathbf{M}_2$ for the forces and moments exerted at $\bar{X}^2$ of $\mathcal{V}_2$. The expressions for these conservative forces and moments can be inferred from (S.24) by repositioning the point X_A^1 and X_A^2 at the centers of mass of the respective bodies.

5.1 Infinitesimal relative motions

Now, consider the pairs of configurations $(\boldsymbol{\kappa}_{1,t}, \boldsymbol{\kappa}_{2,t})$ and $(\boldsymbol{\kappa}_{1,t'}, \boldsymbol{\kappa}_{2,t'})$ of two rigid bodies (cf. Fig. 4). We distinguish quantities associated with $\boldsymbol{\kappa}_{K,t'}$ with a superscript $'$ and assume that the pairs of configurations differ by an infinitesimal rigid body motion. Thus,

$$\Delta\mathbf{y}_A = \mathbf{y}'_A - \mathbf{y}_A = O(\epsilon),$$

$$\mathbf{I} + \Delta\mathbf{R} = \mathbf{R}'\mathbf{R}^T, \qquad \Delta\mathbf{R} = O(\epsilon), \tag{S.25}$$

where ϵ is a small number, $\mathbf{I}$ is the identity tensor, and $\Delta\mathbf{R}$ is a skew-symmetric tensor with an associated axial vector $\Delta\boldsymbol{\beta}$:

$$\Delta\mathbf{R}\mathbf{a} = \Delta\boldsymbol{\beta} \times \mathbf{a}, \tag{S.26}$$

for any vector $\mathbf{a}$. The vector $\Delta\boldsymbol{\beta}$ is known as the rotation vector:

$$\Delta\boldsymbol{\beta} = \sum_{i=1}^{3} \left((\beta_{i'} - \beta_i)\, \tilde{\mathbf{g}}_i \right) + O(\epsilon^2). \tag{S.27}$$

The skew-symmetry of $\Delta\mathbf{R}$ is synonymous with the fact that the relative rotation $\mathbf{R}'\mathbf{R}^T$ is infinitesimal (see [21]). In (S.27), $\beta_{i'}$ are the values of the Euler angles for $\mathbf{R}'$ and β_i are the values of the Euler angles for the rotation $\mathbf{R}$ (cf. (S.22)).

These changes in configuration produce changes in the forces and moments acting on the bodies:

$$\left(\mathbf{F}_2^A\right)' = -\left(\mathbf{F}_1^A\right)' = \mathbf{F}_2^A + \Delta\mathbf{F}_2^A,$$

$$\left(\mathbf{M}_2^A\right)' = -\left(\mathbf{M}_1^A\right)' = \mathbf{M}_2^A + \Delta\mathbf{M}_2^A. \tag{S.28}$$

5.2 Cartesian stiffness matrix K^c

The increments in forces $\Delta\mathbf{F}_K^A$ and moments $\Delta\mathbf{M}_K^A$ associated with the infinitesimal displacement and rotation vectors, $\Delta\mathbf{y}_A$ and $\Delta\boldsymbol{\beta}$, are used to define several distinct stiffness matrices relating changes in the Cartesian components of the pair of forces and moments to small relative displacements and rotations between the rigid bodies. As emphasized in the literature (see [2,4,8,9,11,12,18,19] and references therein) the specific stiffness matrix depends on which bases are used to compute the increments in force, moment, displacement, and rotation.

To continue, it is convenient to first introduce the generalized Cartesian displacement and force arrays:

$$\Delta\left({}^c\mathsf{y}_A\right) = \begin{bmatrix} \Delta\mathbf{y}_A \cdot \mathbf{E}_1 \\ \Delta\mathbf{y}_A \cdot \mathbf{E}_2 \\ \Delta\mathbf{y}_A \cdot \mathbf{E}_3 \\ \Delta\boldsymbol{\beta} \cdot \mathbf{E}_1 \\ \Delta\boldsymbol{\beta} \cdot \mathbf{E}_2 \\ \Delta\boldsymbol{\beta} \cdot \mathbf{E}_3 \end{bmatrix}, \quad \Delta\left({}^c\mathsf{F}_K^A\right) = \begin{bmatrix} \left(\Delta\mathbf{F}_K^A\right) \cdot \mathbf{E}_1 \\ \left(\Delta\mathbf{F}_K^A\right) \cdot \mathbf{E}_2 \\ \left(\Delta\mathbf{F}_K^A\right) \cdot \mathbf{E}_3 \\ \left(\Delta\mathbf{M}_K^A\right) \cdot \mathbf{E}_1 \\ \left(\Delta\mathbf{M}_K^A\right) \cdot \mathbf{E}_2 \\ \left(\Delta\mathbf{M}_K^A\right) \cdot \mathbf{E}_3 \end{bmatrix}. \tag{S.29}$$

Using these arrays, we can define the Cartesian stiffness matrix K^c:

$$\Delta\left({}^c\mathsf{F}_2^A\right) = -\Delta\left({}^c\mathsf{F}_1^A\right) = -\mathsf{K}^c \Delta\left({}^c\mathsf{y}_A\right) + O\left(\epsilon^2\right), \tag{S.30}$$

From [12], the stiffness matrix K^c in (S.30) has components given by

$$\mathsf{K}^c = \begin{bmatrix} \mathsf{I} & \mathsf{0} \\ \mathsf{0} & {}^E\tilde{\mathsf{T}}^T \end{bmatrix} \underbrace{\begin{bmatrix} \mathsf{H}^1 & \mathsf{H}^3 \\ (\mathsf{H}^3)^T & \mathsf{H}^2 \end{bmatrix}} \begin{bmatrix} \mathsf{I} & \mathsf{0} \\ \mathsf{0} & {}^E\tilde{\mathsf{T}} \end{bmatrix} + \begin{bmatrix} \mathsf{0} & \mathsf{0} \\ \mathsf{0} & \mathsf{D} \end{bmatrix}, \tag{S.31}$$

where, the underbraced term is the Hessian H of the potential energy function U with

$$\mathsf{H}^1_{ij} = \frac{\partial^2 U}{\partial Y_i \partial Y_j}, \qquad \mathsf{H}^2_{ij} = \frac{\partial^2 U}{\partial \beta_i \partial \beta_j}, \qquad \mathsf{H}^3_{ij} = \frac{\partial^2 U}{\partial \beta_i \partial Y_j}, \tag{S.32}$$

the matrix ${}^E\tilde{\mathsf{T}}$ has components $({}^E\tilde{T})_{ij} = \tilde{\mathbf{g}}^i \cdot \mathbf{E}_j$ and the components of D are given by[3]

$$D_{pq} = \sum_{i=1}^{3} \sum_{r=1}^{3} \left(\frac{\partial ({}^E\tilde{T})_{ip}}{\partial \beta_r} ({}^E\tilde{T})_{rq} \frac{\partial U}{\partial \beta_i} \right). \tag{S.33}$$

Notice that even though the Hessian H is symmetric, K^c is not necessarily symmetric due to the possible prestress (i.e., $\mathsf{D} \neq \mathsf{0}$) and the use of Euler angles to parameterize the rotation $\mathbf{R}$ (i.e., ${}^E\tilde{\mathsf{T}} \neq \mathsf{I}$).

Various other Cartesian stiffness matrices can also be defined depending on the variables used to parameterize the potential energy function U of the system. These are elaborated upon in further detail in [12].

[3] For $\mathbf{R}$ where $\mathbf{Q}_1 = \mathbf{I}$, the ${}^E\tilde{\mathsf{T}}$ matrix for the 1-2-3 Euler angle sequence is given by (S.17).

6 Related stiffness matrices

We now turn to showing how the Cartesian stiffness matrix is related to some other stiffness matrices that have appeared in the spinal mechanics literature.

6.1 Experimental stiffness matrices

Frequently, experimental determinations of the stiffness matrix elements associated with the intervertebral joint have involved pairs of vertebral bodies. Most commonly, the lower vertebra is fixed, the upper vertebra subjected to infinitesimal motion, and the forces and moments due to the ensuing deformation measured [6,7,22,23]. Alternatively, a force or moment is applied and the resulting deformations measured [5,17]. Variations of these protocols have also been tested using larger deformations [15].

The elements of the experimental stiffness matrix are then determined by comparing changes in the forces and moments to the relative motion between the upper and lower vertebra. Depending on how these quantities are characterized, there are several possible definitions of the stiffness matrix. For example, if the increments in loads and displacements are expressed as

$$\Delta\tilde{\mathsf{y}}_A = \begin{bmatrix} \Delta\mathbf{y}_A\cdot\mathbf{e}_1^1 \\ \Delta\mathbf{y}_A\cdot\mathbf{e}_2^1 \\ \Delta\mathbf{y}_A\cdot\mathbf{e}_3^1 \\ \Delta\boldsymbol{\beta}\cdot\tilde{\mathbf{g}}^1 \\ \Delta\boldsymbol{\beta}\cdot\tilde{\mathbf{g}}^2 \\ \Delta\boldsymbol{\beta}\cdot\tilde{\mathbf{g}}^3 \end{bmatrix}, \qquad \Delta\mathsf{F}_K^A = \begin{bmatrix} \left(\Delta\mathbf{F}_K^A\right)\cdot\mathbf{e}_1^1 \\ \left(\Delta\mathbf{F}_K^A\right)\cdot\mathbf{e}_2^1 \\ \left(\Delta\mathbf{F}_K^A\right)\cdot\mathbf{e}_3^1 \\ \left(\Delta\mathbf{M}_K^A\right)\cdot\tilde{\mathbf{g}}_1 \\ \left(\Delta\mathbf{M}_K^A\right)\cdot\tilde{\mathbf{g}}_2 \\ \left(\Delta\mathbf{M}_K^A\right)\cdot\tilde{\mathbf{g}}_3 \end{bmatrix}, \tag{S.34}$$

then we can write

$$\Delta\mathsf{F}_2^A = -\mathsf{K}^E\Delta\mathsf{y}_A. \tag{S.35}$$

In experimental situations, the lower vertebra is frequently fixed and this simplifies the calculation of K^E. First, the basis vectors $\{\mathbf{e}_1^1,\mathbf{e}_2^1,\mathbf{e}_3^1\}$ are equivalent to the set of fixed Cartesian basis vectors $\{\mathbf{E}_1,\mathbf{E}_2,\mathbf{E}_3\}$ and the force and displacement components featured in (S.34) equal those in (S.29). This is especially convenient as the components of this stiffness matrix featuring in (S.35) can now be easily related to those featuring in (S.31).

Measurements of the stiffness matrix K^E of an intervertebral joint are presented in [15]. These authors found that K^E is generally not symmetric. This lack of symmetry can be attributed to a variety of factors among them large rotations of the joint and nonconservative forces and moments in the joint.

In [3], we argue that K^E can be thought of as an approximation of the Hessian H of the potential energy function U. This is valid as the motions used the determine the components of K^E are often uniaxial and infinitesimal [22]). Hence,

$${}^E\tilde{\mathsf{T}} \approx \mathsf{I}, \qquad \mathsf{D} \approx \mathsf{0}. \tag{S.36}$$

Even when the motion does not strictly satisfy these conditions, the standards deviations in the stiffness matrix components are usually so large that it is still reasonable to assume that $\mathsf{K}^E \approx \mathsf{H}$. In fact, K^E and H are often used interchangeably in the spinal literature on the subject. This is one of the underlying assumptions behind the symmetrization of the experimental stiffness matrices reported in, for example, [7] and [17].[4]

6.2 Bushing stiffness matrix K^B

Typical bushing stiffness matrices K^B are defined as the diagonal of the Hessian H of an appropriate potential energy function U. The basis vectors for the bushing forces and moments are those featured in the expression for $\Delta\mathsf{F}_K^A$ given by $(\text{S.34})_2$. In [3], this stiffness matrix is modified to incorporate all 36 elements of a 6×6 stiffness matrix hence permitting the analysis of coupled motion. The reader is also referred to this work for details on the generalized displacement array used to define K^B.

6.3 The stiffness matrix K^D

In [15], the moments $\mathbf{M}_K^A$ are expressed in the Euler basis. Hence, the stiffness matrix K^D presented in this work is

$$\bar{\Delta}\mathsf{F}_2^A = -\bar{\Delta}\mathsf{F}_1^A = -\mathsf{K}^D\Delta\mathsf{y}_A + O\left(\epsilon^2\right), \tag{S.37}$$

where

$$\bar{\Delta}\mathsf{F}_K^A = \begin{bmatrix} \left(\Delta\mathbf{F}_K^A\right)\cdot\mathbf{E}_1 \\ \left(\Delta\mathbf{F}_K^A\right)\cdot\mathbf{E}_2 \\ \left(\Delta\mathbf{F}_K^A\right)\cdot\mathbf{E}_3 \\ \left(\Delta\mathbf{M}_K^A\right)\cdot\tilde{\mathbf{g}}_1 \\ \left(\Delta\mathbf{M}_K^A\right)\cdot\tilde{\mathbf{g}}_2 \\ \left(\Delta\mathbf{M}_K^A\right)\cdot\tilde{\mathbf{g}}_3 \end{bmatrix}. \tag{S.38}$$

[4] We note that additional symmetry restrictions based on the anatomy of the intervertebral joint are also imposed on the stiffness matrices featured in these references. These symmetries result in a stiffness matrix with 12 independent components and the banded structure of this matrix is identical to that in the stiffness matrix K_F^E that is used in Section 5.1 of [3].

The components of the stiffness matrix can be related to the Hessian of a potential energy function with the help of (S.10) and (S.31):

$$\mathsf{K}^D = \begin{bmatrix} \mathsf{H}^1 & \mathsf{H}^3 \\ (\mathsf{H}^3)^T & \mathsf{H}^2 \end{bmatrix} + \begin{bmatrix} 0 & 0 \\ 0 & \mathsf{D}^E\tilde{\mathsf{T}}^{-1} \end{bmatrix}. \tag{S.39}$$

We note for completeness that the preload term $\mathsf{D}^E\tilde{\mathsf{T}}^{-1}$ is erroneously absent from the expression for the stiffness matrix $\mathbf{K}_u$ in equation (B9) in [15]. This omission does not affect the other results in their paper.

Acknowledgements

Maurice Curtin's work was supported by Enterprise Ireland and a bursary from University College Dublin, while the four other coauthors' work was partially supported by the National Science Foundation of the United States under Grant No. CMMI 0726675.

References

1. Andriacchi, T.P., Mikosz, R.P., Hampton, S.J., Galante, J.O.: Model studies of the stiffness characteristics of the human knee joint. Journal of Biomechanics **16**(1), 23–29 (1983). DOI 10.1016/0021-9290(83)90043-X
2. Chen, S.F., Kao, I.: Conservative congruence transformation for joint and cartesian stiffness matrices of robotic hands and fingers. The International Journal of Robotics Research **19**(9), 835–847 (2000). DOI 10.1177/02783640022067201
3. Christophy, M., Curtin, M., Faruk Senan, N.A., Lotz, J.C., O'Reilly, O.M.: On the modeling of the intervertebral joint in multibody models for the spine. Multibody System Dynamics **30**(4), 413–432 (2013). DOI 10.1007/s11044-012-9331-x. URL http://dx.doi.org/10.1007/s11044-012-9331-x
4. Ciblak, N., Lipkin, H.: Asymmetric Cartesian stiffness for the modelling of compliant robotic systems. In: G.R. Pennock, J. Angeles, E.F. Fichter, R.A. Freeman, H. Lipkin, B.S. Thompson, J. Wiederrich, G.L. Wiens (eds.) Robotics: Kinematics, Dynamics and Controls. Presented at The 1994 ASME Design Technical Conferences - 23rd Biennial Mechanisms Conference, Minneapolis, Minnesota, September 11–14, 1994, vol. DE-72, pp. 197–204 (1994)
5. Crisco, J.J., Fujita, L., Spenciner, D.: The dynamic flexion/extension properties of the lumbar spine in vitro using a novel pendulum system. Journal of Biomechanics **40**(12), 2767–2773 (2007). DOI 10.1016/j.jbiomech.2006.12.013
6. Gardner-Morse, M.G., Stokes, I.A.F.: Physiological axial compressive preloads increase motion segment stiffness, linearity and hysteresis in all six degrees of freedom for small displacements about the neutral posture. Journal of Orthopaedic Research **21**(3), 547–552 (2003)
7. Gardner-Morse, M.G., Stokes, I.A.F.: Structural behavior of the human lumbar spinal motion segments. Journal of Biomechanics **37**(2), 205–212 (2004). DOI 10.1016/j.jbiomech.2003.10.003
8. Griffis, M., Duffy, J.: Global stiffness modeling of a class of simple compliant couplings. Mechanism and Machine Theory **28**(2), 207–224 (1993). DOI 10.1016/0094-114X(93)90088-D
9. Howard, S., Žefran, M., Kumar, V.: On the 6 × 6 Cartesian stiffness matrix for three-dimensional motions. Mechanism and Machine Theory **33**(4), 389–408 (1998). DOI 10.1016/S0094-114X(97)00040-2
10. Kane, T.R., Likins, P.W., Levinson, D.A.: Spacecraft Dynamics. McGraw-Hill, New York (1983)
11. Kövecses, J., Angeles, J.: The stiffness matrix in elastically articulated rigid-body systems. Multibody System Dynamics **18**(2), 169–184 (2007). DOI 10.1007/s11044-007-9082-2
12. Metzger, M.F., Faruk Senan, N.A., O'Reilly, O.M.: On Cartesian stiffness matrices in rigid body dynamics: an energetic perspective. Multibody System Dynamics **24**(4), 441–472 (2010). DOI 10.1007/s11044-010-9205-z
13. O'Reilly, O.M.: The dual Euler basis: Constraints, potentials, and Lagrange's equations in rigid body dynamics. ASME Journal of Applied Mechanics **74**(2), 256–258 (2007). DOI 10.1115/1.2190231
14. O'Reilly, O.M.: Intermediate Engineering Dynamics: A Unified Approach to Newton-Euler and Lagrangian Mechanics. Cambridge University Press, New York (2008)
15. O'Reilly, O.M., Metzger, M.F., Buckley, J.M., Moody, D.A., Lotz, J.C.: On the stiffness matrix of the intervertebral joint: Application to total disk replacement. ASME Journal of Biomechanical Engineering **131**, 081,007–1–081,007–9 (2009). DOI 10.1115/1.3148195
16. O'Reilly, O.M., Srinivasa, A.R.: On potential energies and constraints in the dynamics of rigid bodies and particles. Mathematical Problems in Engineering. Theory, Methods and Applications **8**(3), 169–180 (2002). DOI 10.1080/10241230215286
17. Panjabi, M.M., Brand Jr., R.A., White III, A.A.: Three-dimensional flexibility and stiffness properties of the human thoracic spine. Journal of Biomechanics **9**(4), 185–192 (1976). DOI 10.1016/0021-9290(76)90003-8
18. Pigoski, T., Griffis, M., Duffy, J.: Stiffness mappings employing different frames of reference. Mechanism and Machine Theory **33**(6), 825–838 (1998). DOI 10.1016/S0094-114X(97)00083-9
19. Quennouelle, C., Gosselin, C.M.: Stiffness matrix of compliant parallel mechanisms. In: Advances in Robot Kinematics: Analysis and Design, pp. 331–341 (2008). DOI 10.1007/978-1-4020-8600-7-35
20. Shabana, A.A.: Computational Dynamics, 3 edn. John Wiley & Sons Inc., New York (2010)
21. Shuster, M.D.: A survey of attitude representations. Journal of the Astronautical Sciences **41**(4), 439–517 (1993)
22. Stokes, I.A.F., Gardner-Morse, M.G., Churchill, D., Laible, J.P.: Measurement of a spinal motion segment stiffness matrix. Journal of Biomechanics **35**(4), 517–521 (2002)
23. Stokes, I.A.F., Iatridis, J.C.: Basic Orthopaedic Biomechanics and Mechano-Biology, third edn., chap. Biomechanics of the Spine, pp. 529–561. Lippincott Williams & Wilkins, Philadelphia (2005). Edited by Mow, V. C. and Huiskes, R.